Separation of Several Aliased Images to Increase Volume Speed

Daniel B. Rowe[1,2]
[1]Department of Mathematics, Statistics and Computer Science, Marquette University
[2]Department of Biophysics, Medical College of Wisconsin

Abstract

In functional MRI, each slice in a volume is traditionally excited individually, measuring enough data in a single k-space array to reconstruct an image for that slice. Over the last decade, techniques have been developed to sample less data within an image thus decreasing the acquisition time for an image of each slice. However, a new thrust is to simultaneously excite multiple slices that make up a volume and sample sufficient data in a single k-space array to represent multiple slices. This single array of k-space data can be reconstructed into a single image representing the aliased slices, and then separated into individual images for each slice. A technique and statistical description has been presented for aliasing and separating two complex-valued slices with a single coil image. The thrust of this work is to extend that work to separate complex-valued images for a higher numbers of aliased slices and present statistical implications.

Key Words: MRI, fMRI, parallel slice, multiband, image reconstruction, magnetic resonance imaging

1. Introduction

In functional magnetic resonance imaging (fMRI), an image volume is generally made up of slices of images. The cognitively functioning brain changes rapidly and a volume of image slices takes on the order of a second when complete image spatial frequency data is measured. Since parallel imaging was conceived (1), methods such as SENSE (2) and GRAPPA (3) or their variants have greatly contributed to the in-plane acceleration of images using multicoil arrays to subsample spatial frequency lines and reconstruct an image of a single slice. Recent research efforts have been focused on the simultaneous excitation and acquisition of multiple parallel images of slices to build up a single volume.

Initial work on the topic involved the acquisition of images of two simultaneously excited slices in two experiments with a single channel coil (4, 5), which was extended to multiple slices using multiple channel coils in a single experiment (6, 7), and to two encoded slices using a single channel quadrature coil (7, 8, 9). Here a new complex-valued approach for acquiring a single complex-valued image of multiple slices and separating multiple complex-valued images of slices using a multiple channel coil array is described. The recent line of research for increased biological information utilizing complex-valued images and magnitude-phase time series models to compute fMRI activation (10, 11, 12) provides the motivation to separate complex-valued images.

The outline of this manuscript is as follows: The Background section will describe coil arrays and the image aliasing process. The Methods section describes the multiple aliased image separation approach and the statistical properties of the separated images including

their expected mean, variance, and correlation structure. The Results section presents Monte Carlo simulated data. Finally, the Discussion and Conclusion section discusses the presented methods and comments on image separation.

2. Background

In fMRI, a multiple channel coil arrays consist of multiple coil elements generally distributed within a cylindrical shell about the head. The sensitivity of a given coil to tissue within a slice being imaged depends upon the distance from the center of the coil. Each coil element has a different sensitivity to a given region being imaged.

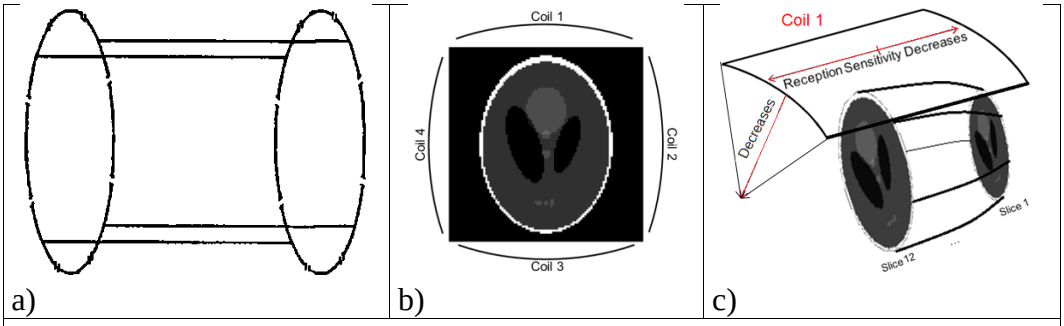

Figure 1: A 4-channel birdcage coil array a) side view, b) axial view with Shepp-Logan phantom slice in it, c) angled view of a single coil element with two slices of a Shepp-Logan phantom in it where decreasing coil sensitivities are depicted.

2.1 Coil Arrays

A common fMRI coil orientation is what is what is referred to as a "birdcage" due to its cylindrical arrangement. A side view illustration of a 4-channel array is given in Figure 1a and an axial view of a 4-channel coil with a Shepp-Logan phantom brain slice is

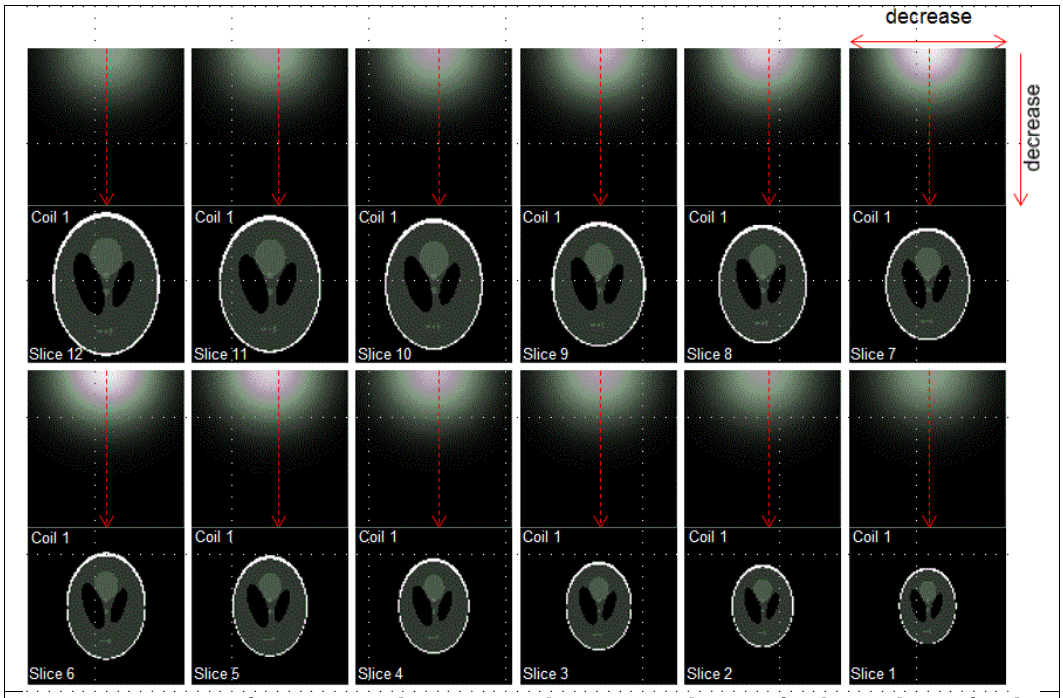

Figure 2: Depiction of sensitivities decreasing with increasing distance for the 12 slices of coil 1.

presented in Figure 1b. The sensitivity that a given coil has to receive a signal in a particular location in a slice depends upon the distance the slice is along the axis of the cylinder from the center of the coil and the distance the location is radially from the center of the coil as depicted in Figure 1c.

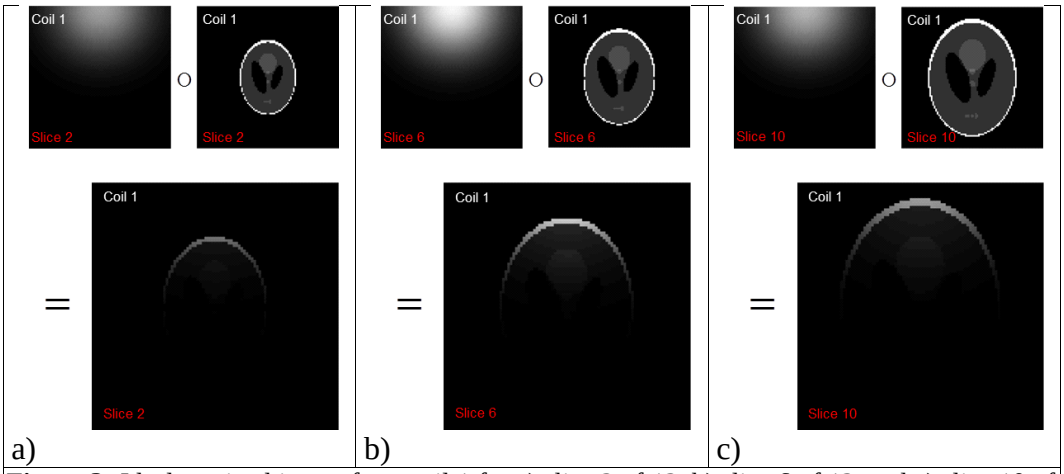

Figure 3: Ideal received image from coil 1 for a) slice 2 of 12, b) slice 6 of 12, and c) slice 10 of 12.

When there are for example a total of N_z=12 slices to make up the volume to be imaged, the coil sensitivity is decreased for slices further from the center of the coil and within a slice away from the center of the coil. This decrease in coil sensitivity is illustrated for coil 1 in Figure 2. Similar decreases in coil sensitivities exist for the remaining coils.

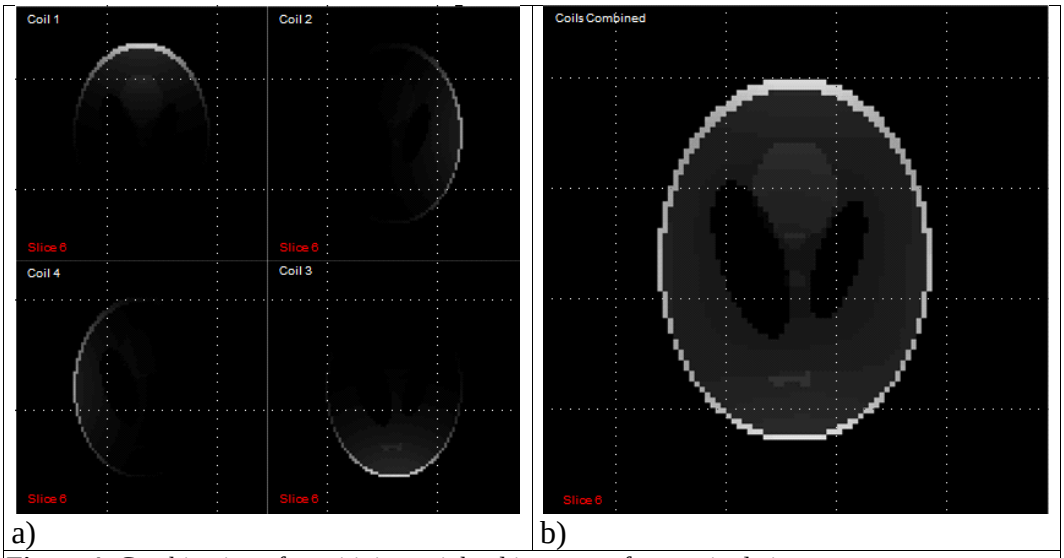

Figure 4: Combination of sensitivity weighted images to form a single image.

For a given slice being imaged, each coil produces an image that is the product of the coil sensitivity and the signal from the object being imaged. This sensitivity of the received signal is shown in Figure 3 for slices 2, 6, and 10 of coil 1 where "○" denotes the Hadamard product point-wise multiplying the elements in two arrays. Note that the image does not completely show the object and that the representation of the object fades further away from the center of the coil.

For a given slice, the four sensitivity weighted images as depicted in Figure 4a for slice 6 of 12 are combined to form a single image. The combination of four sensitivity weighted images for slice 6 is depicted in Figure 4b for slice 6 of 12.

New techniques have been and are being developed to simultaneously encode a packet of several slices, measure an image that is sensitivity weighted sum of the images in the packet (aliased image), and reconstruct individual images of the slices in the packet.

2.2 Image Aliasing

To illustrate the process of aliasing sensitivity weighted slices, imagine that there are N_S=12 slices being imaged as in the second and fourth rows of Figure 2. The N_S=12 consecutively numbered axial slices from superior to inferior can be grouped into for example N_P=4 packets of N_A=3 if we are aliasing 3 slices. If we denote the jth packet as P_j, then we can group packets as P_1={1,5,9}, P_2={2,6,10}, P_3={3,7,9}, and P_4={4,8,12}.

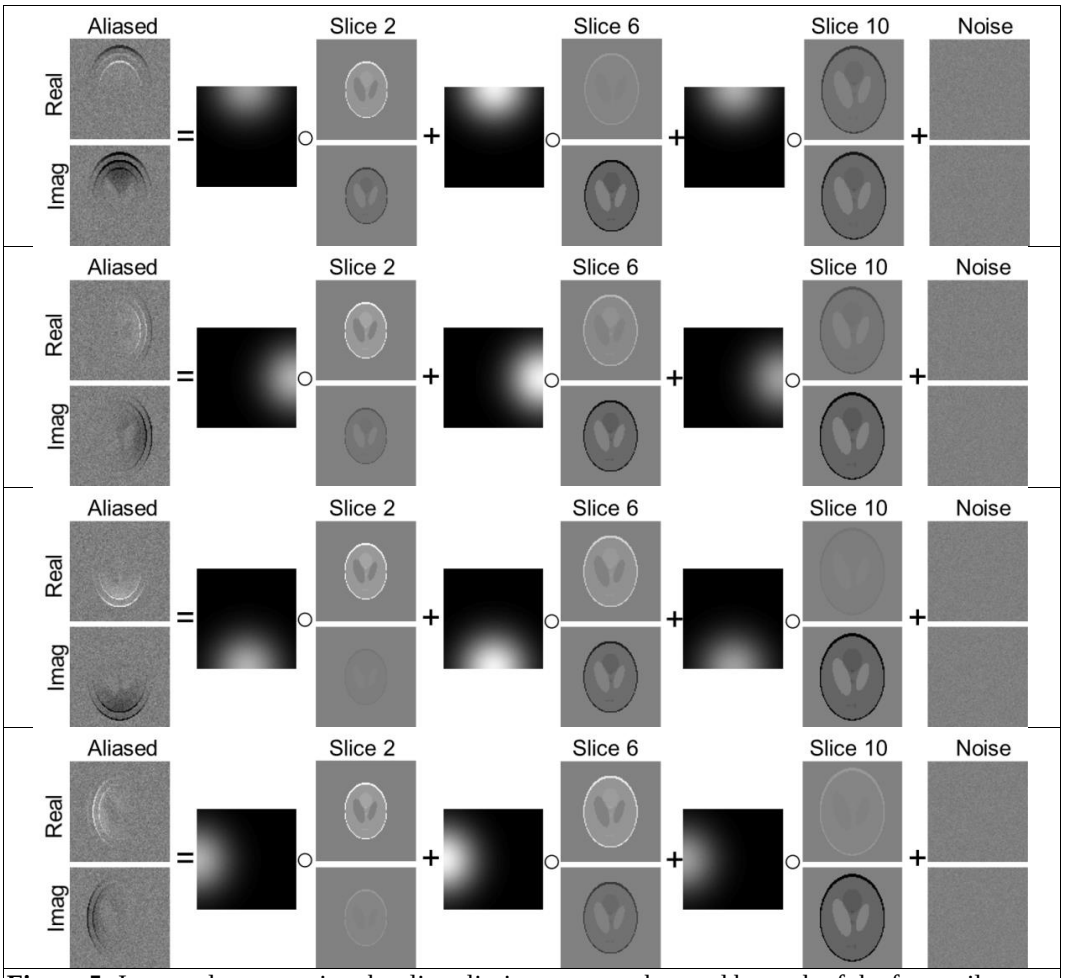

Figure 5: Images demonstrating the slice aliasing process observed by each of the four coils.

Using packet 2 as an example, the noiseless sensitivity weighted aliasing of the N_A=3 slices using N_C=4 coils is visually depicted in Figure 5. The sensitivity weighted sum of the N_A=3 slices is seen in Figure 5a for coil 1, in Figure 5b for coil 2, in Figure 5c for coil 3, and in Figure 5d for coil 4. Note that no coil has complete sensitivity to the entire object within the slices.

The observed values within each of the voxels in the aliased image for coil j is described as the sensitivity weighted sum of the true mean values of each slice plus measurement error. For coil j, the observed value in a given voxel can be represented as

$$(y_{jR} + iy_{jI}) = \sum_k S_{j,k}(\rho_k \cos\theta_k + i\rho_k \sin\theta_k) + (\varepsilon_{jR} + i\varepsilon_{jI}) \quad (1)$$

where y_{jR} and y_{jI} are the observed aliased real and imaginary parts, $S_{j,k}$ is the sensitivity of coil j in slice k, ρ_k is the true magnitude in slice k, θ_k is the true phase in slice k, while ε_{jR} and ε_{jI} are the real and imaginary additive error terms.

For the illustrative example where the N_A=3 slices of 2, 6, and 10 are aliased for N_C=4 coils, the aliasing process for a given observed voxel value by coil j=1,..,4 is given by

$$\begin{aligned}(y_{jR} + iy_{jI}) &= S_{j,2}(\rho_2 \cos\theta_2 + i\rho_2 \sin\theta_2) \\ &+ S_{j,6}(\rho_6 \cos\theta_6 + i\rho_6 \sin\theta_6) \\ &+ S_{j,10}(\rho_{10} \cos\theta_{10} + i\rho_{10} \sin\theta_{10}) \\ &+ (\varepsilon_{jR} + i\varepsilon_{jI})\end{aligned} \quad (2)$$

which can be written in terms of vectors and matrices for all coils as

$$\begin{pmatrix} y_{1R} \\ y_{2R} \\ y_{3R} \\ y_{4R} \\ y_{1I} \\ y_{2I} \\ y_{3I} \\ y_{4I} \end{pmatrix} = \begin{pmatrix} S_{1,2} & S_{1,6} & S_{1,10} & 0 & 0 & 0 \\ S_{2,2} & S_{2,6} & S_{2,10} & 0 & 0 & 0 \\ S_{3,2} & S_{3,6} & S_{3,10} & 0 & 0 & 0 \\ S_{4,2} & S_{4,6} & S_{4,10} & 0 & 0 & 0 \\ 0 & 0 & 0 & S_{1,2} & S_{1,6} & S_{1,10} \\ 0 & 0 & 0 & S_{2,2} & S_{2,6} & S_{2,10} \\ 0 & 0 & 0 & S_{3,2} & S_{3,6} & S_{3,10} \\ 0 & 0 & 0 & S_{4,2} & S_{4,6} & S_{4,10} \end{pmatrix} \begin{pmatrix} \rho_2 \cos\theta_2 \\ \rho_6 \cos\theta_6 \\ \rho_{10} \cos\theta_{10} \\ \rho_2 \sin\theta_2 \\ \rho_6 \sin\theta_6 \\ \rho_{10} \sin\theta_{10} \end{pmatrix} + \begin{pmatrix} \varepsilon_{1R} \\ \varepsilon_{2R} \\ \varepsilon_{3R} \\ \varepsilon_{4R} \\ \varepsilon_{1I} \\ \varepsilon_{2I} \\ \varepsilon_{3I} \\ \varepsilon_{4I} \end{pmatrix} \quad (3)$$

and more compactly as

$$\begin{pmatrix} y_{AR} \\ y_{AI} \end{pmatrix} = \begin{pmatrix} S & 0 \\ 0 & S \end{pmatrix} \begin{pmatrix} \beta_R \\ \beta_I \end{pmatrix} + \begin{pmatrix} \varepsilon_{AR} \\ \varepsilon_{AI} \end{pmatrix} \quad (4)$$

or in the familiar form as

$$y_A = X_A \beta + \varepsilon_A \quad (5)$$

where y_R=(y_{1R},y_{2R},y_{3R},y_{4R})', y_I=(y_{1I},y_{2I},y_{3I},y_{4I}) ', X_A=$I_2 \otimes S$, and β_R=(β_R, β_I)' while the mean and covariance of the measurement error are $E(\varepsilon_A)$=0 and $cov(\varepsilon_A)$=Ψ. The "design" matrix X_A in Equation 5 is severely rank deficient, rank(X_A)≥2, and thus we can't invert it or X_A 'X_A for least squares estimation.

3. Methods

Since we can't separate the images solely based upon the data that we have from the experiment, we need additional information. We can acquire complete nonaliased calibration images of the slices within each packet for each coil and utilize these for image separation.

3.1 Image Separation

Full images of the each of the slices that make up the volume image are acquired. To illustrate the image separation, the example of 12 slices that are allocated to four packets of three will be continued with particular attention to packet 2 with slices 2, 6, and 10.

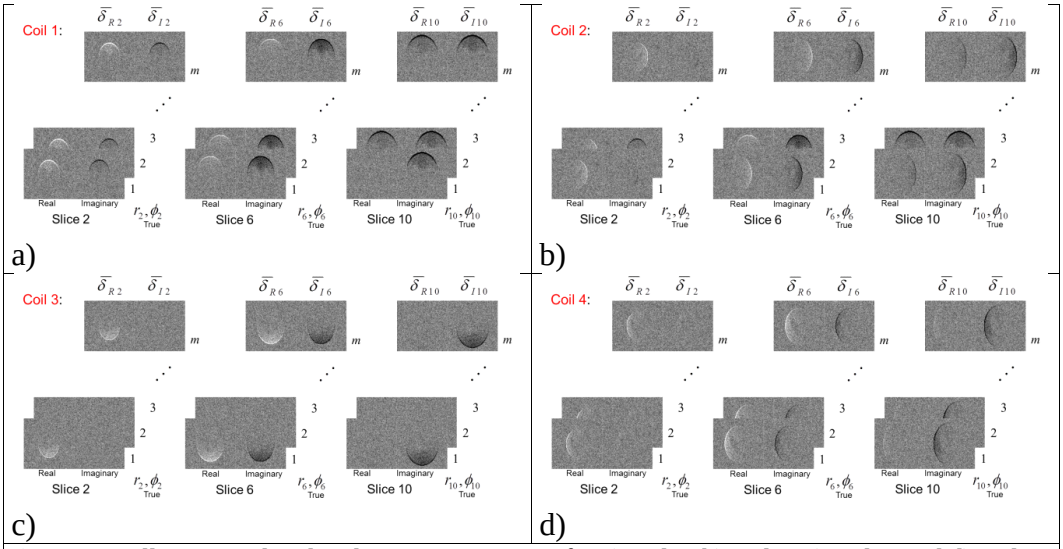

Figure 6: Fully acquired real and imaginary images for a) coil 1, b) coil 2, c) coil 3, and d) coil 4.

In Figure 6 are *m* fully acquired real and imaginary images of slices 2, 6, and 10 for each of the coils. Figure 6a are the m images for coil 1, Figure 6b for coil 2, Figure 6c for coil 3, and Figure 6d for coil 4. In each of the four subfigures in Figure 6, the *m* images are averaged for both real and imaginary of each of the coils represented as $\bar{\delta}$'s to form reference calibration images.

Utilizing slice 6 in the example with 12 slices in 4 packets of 3, we can form the magnitude of the reference calibration images as depicted in Figure 7a, and divide each of them by the magnitude of the complex sum of the coil images as represented in Figure 7b. This is done for each slice to produce coil sensitivities as represented in Figure 7c. This process is repeated for each of the N_Z slices. In each voxel, the real and imaginary parts of the fully acquired reference calibration images $\bar{\delta}_R = (\bar{\delta}_{R2}, \bar{\delta}_{R6}, \bar{\delta}_{R10})'$ and $\bar{\delta}_I = (\bar{\delta}_{I2}, \bar{\delta}_{I6}, \bar{\delta}_{I10})'$ are artificially aliased as in Equation 6

$$\begin{pmatrix} \nu_{AR} \\ \nu_{AI} \end{pmatrix} = \begin{pmatrix} C & 0 \\ 0 & C \end{pmatrix} \begin{pmatrix} \bar{\delta}_R \\ \bar{\delta}_I \end{pmatrix} \tag{6}$$

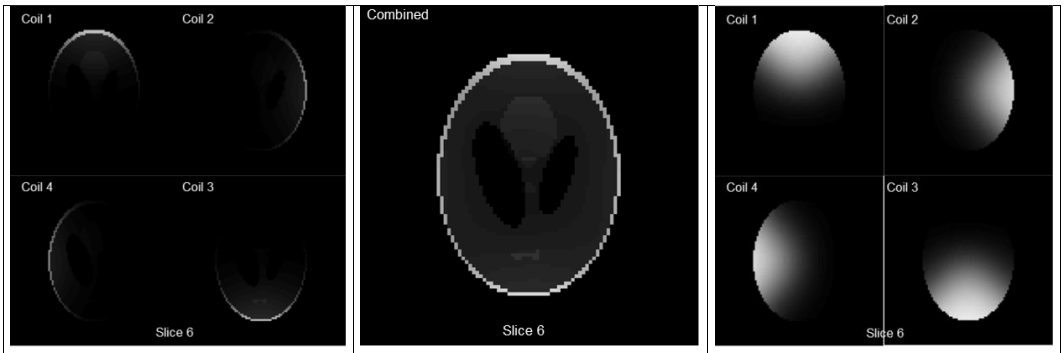

Figure 7: Images for slice 6 of a) magnitude of reference calibration images for each of the four coils, b) magnitude of sum of complex-valued coil images, c) sensitivities for each of the four coils (image a divided by image b).

with the use of a contrast aliasing matrix C to form the artificially aliased image values $\nu_R = (\nu_{R1}, \nu_{R2}, \nu_{R3})'$ and $\nu_I = (\nu_{I1}, \nu_{I2}, \nu_{I3})'$ that are utilized for separating the images of the N_A slices where

$$C = \begin{pmatrix} -1 & 0 & 1 \\ 1 & -2 & 1 \end{pmatrix}. \tag{7}$$

The model in Equation 4 can be combined with the new artificially aliased images and represented as

$$\begin{pmatrix} y_{AR} \\ \nu_{AR} \\ y_{AI} \\ \nu_{AI} \end{pmatrix} = \begin{pmatrix} S & 0 \\ C & 0 \\ 0 & S \\ 0 & C \end{pmatrix} \begin{pmatrix} \beta_R \\ \beta_I \end{pmatrix} + \begin{pmatrix} \varepsilon_{AR} \\ \eta_{AR} \\ \varepsilon_{AI} \\ \eta_{AR} \end{pmatrix} \tag{8}$$

where η_R and η_I are error terms for the newly aliased images. We can see that due to our selection C is of rank (N_A-1) which is 2 in this example, and S is at least of rank 1. Thus Equation 8 can now be represented in the more familiar form

$$y = X\beta + \varepsilon. \tag{9}$$

So we can separate the images of the N_A slices by estimating β as

$$\hat{\beta} = (X'\Psi^{-1}X)^{-1}X'\Psi^{-1}y. \tag{10}$$

This technique for separating the images of the slices is a generalization of the method of Rowe (13, 14).

3.2 Separated Statistics

It is important to examine the separated images to fully understand their statistical properties in terms of mean, variance, and correlation. If we denote the mean and

covariance of the reference calibration images as $E(\bar{\delta}) = \delta$ and $\text{cov}(\bar{\delta}) = \Gamma$, then it can be shown that the mean and covariance of our separated images are given by

$$E(\hat{\beta}) = \begin{pmatrix} (S'\Psi^{-1}S + C'C)^{-1}(S'\Psi^{-1}S\beta_R + C'C\delta_R) \\ (S'\Psi^{-1}S + C'C)^{-1}(S'\Psi^{-1}S\beta_I + C'C\delta_I) \end{pmatrix} \tag{11}$$

and

$$\text{cov}(\hat{\beta}) = I_2 \otimes (S'\Psi^{-1}S + C'C)^{-1}(S'\Psi^{-1}S)(S'\Psi^{-1}S + C'C)^{-1}. \tag{12}$$

The correlation matrix corr($\hat{\beta}$) can be calculated from the covariance matrix cov($\hat{\beta}$).

More slices can be aliased and separated with the use of larger contrast matrices as given in Table 1. Larger contrast matrices are possible.

Table 1: Contrast matrices for separating aliased slices.

$C_2 = \begin{pmatrix} -1 & 1 \end{pmatrix}$	$C_3 = \begin{pmatrix} -1 & 0 & 1 \\ 1 & -2 & 1 \end{pmatrix}$	$C_4 = \begin{pmatrix} -3 & -1 & 1 & 3 \\ 1 & -1 & 1 & -1 \\ -1 & 3 & -3 & 1 \end{pmatrix}$
$C_5 = \begin{pmatrix} -2 & -1 & 0 & 1 & 2 \\ 2 & -1 & -2 & -1 & 2 \\ -1 & 2 & 0 & -2 & 1 \\ 1 & -4 & 6 & -4 & 1 \end{pmatrix}$	$C_6 = \begin{pmatrix} -5 & -3 & -1 & 1 & 3 & 5 \\ 5 & -1 & -4 & -4 & -1 & 5 \\ -5 & 7 & 4 & -4 & -7 & 5 \\ 1 & -3 & 2 & 2 & -3 & 1 \\ -1 & 5 & -10 & 10 & -5 & 1 \end{pmatrix}$	

4. Results

A simulation was performed in which 50 simulated reference calibration images of slices 2, 6, and 10 of packet 2 were generated as depicted in Figure 6. The first 5 images were

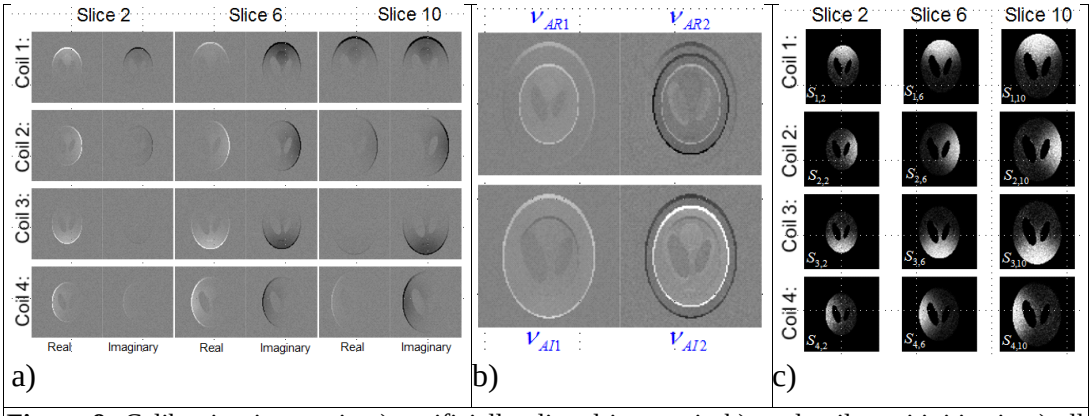

Figure 8: Calibration images in a), artificially aliased images in b), and coil sensitivities in c) all generated from the fully acquired reference calibration images.

deleted to mimic those deleted in experimental fMRI data and the remaining m=45 images were averaged for the final reference calibration images $\bar{\delta}$ as in Figure 8a, for artificially aliased data v in Figure 8b, and for coil sensitivities S in Figure 8c. Note that the anatomical structures of the three slices to be imaged are visually apparent in Figure 8b.

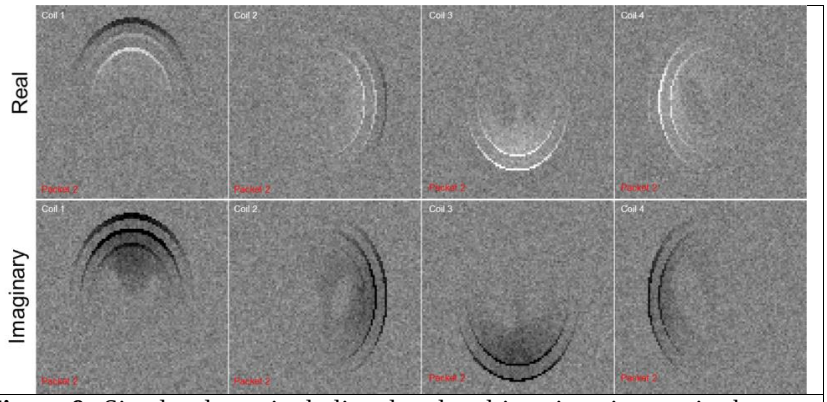

Figure 9: Simulated acquired aliased real and imaginay images in the rows for the four coils in the columns.

The simulation was continued by generating 261 simulated aliased slice images of slices 2, 6, and 10 in packet 2. The first 5 images were deleted to mimic the deletion of the initial images in experimental fMRI data and the remaining n=256 images are to be separated. The first aliased image representing slices 2, 6, and 10 in the second packet that is to be separated is shown in Figure 9. Note in Figure 9 that the rows represent the real and imaginary images while the columns show the images from the four coils.

The aliased images for the four coils can be separated and combined utilizing Equation 10 containing the reference calibration images in Figure 8a, the artificially aliased images in Figure 8b, and the coil sensitivities in Figure 8c. The image separation process was not applied to the aliased images, but the separated images are depicted in Figure 10 where the rows are for slices 2, 6, and 10, and the columns are for real and imaginary. Ideally, in addition to the first aliased image being separated, all n=256 of them can be separated. From separated images, the mean for each separated slice image, the variance, and correlation can be calculated. The sample means, variances, and correlations can be compared to the theoretical values from Equations 11 and 12. The sample values should be very close to the theoretical values.

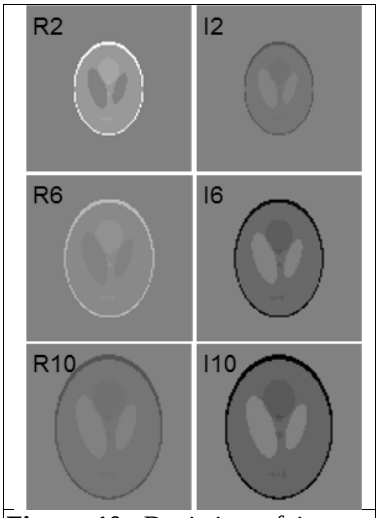

Figure 10: Depiction of images of slices 2, 6, and 10 from separation.

5. Discussion and Conclusions

The multi coil acquisition of fully acquired sensitivity weighted images was described. The N_A slice aliasing process with N_C coils was modeled with coil sensitivities and written in terms of vectors and matrices. Utilizing the reference calibration images, artificially aliased images can be generated using a contrast matrix and coil sensitivities determined. The statistical properties including means, variances, and correlations of the new multi coil multi slice unaliased images are explicitly determined. Simulated data results described but images were not actually unaliased. As the theory implies, any subsampling yields correlated voxels which is an important result. Researchers should be cognizant that artificial correlation can be induced in their data that is of no biological origin merely from image reconstruction.

References

1. Hyde JS, Jesmanowicz A, Froncisz W, Kneeland JB, Grist TM, Campagna NF Parallel image acquisition from noninteracting local coils. J Magn Reson 1986;70:512–517.
2. Pruessmann KP, Weiger M, Scheidegger MB, Boesiger P. SENSE: Sensitivity Encoding for Fast MRI. Magn Reson Med1999;42, 952–962.
3. Griswold MA, Jamob PM, Heidemann RM, Nikkka M, Jellus V, Wang J, Kiefer B, Haase A. Generalized autocalibrating partially parallel acquisition (GRAPPA). Magn Reson Med 2002; 47:1202-1210.
4. Muller S. Multifrequency selective RF pulses for multislice MR imaging. Magn Reson Med 1988;6:364–371.
5. Souza SP, Szumowski J, Dumoulin CL, Plewes DP, Glover G. SIMA: simultaneous multislice acquisition of MR images by Hadamard-encoded excitation. J Comput Assist Tomogr 1988;12:1026–1030.
6. Moeller S, Auerbach E, van de Moortele P-F, Adriany G, Ugurbil K. Functional MRI with 16-fold reduction using multibanded, multisite sampling. Proc Intl Soc Magn Reson Med 2008;16:2366.
7. Jesmanowicz A, Li S-J, Hyde JS. Multi-slice two- and four-fold acceleration with single- and eight-channel coils, respectively. Proc Intl Soc Magn Reson Med 2009;17:1089.
8. Shefchik, DS, Jesmanowicz, A, Budde, M, Nencka, AS. Single-coil two-fold accelerated spin-echo phase-SENSE imaging of the rodent brain at 9.4T. Proc Intl Soc Magn Reson Med 2012, 20:2229.
9. Rowe DB, Hyde JS, Jesmanowicz A, Nencka AS: Separation of two simultaneously encoded slices with a single coil. Proc. Intl. Soc. Magn. Reson. Med., 20:123, 2013.
10. Rowe DB, Logan BR. A complex way to compute fMRI activation. Neuroimage 2004;23:1078–92.
11. Rowe DB. Modeling both the magnitude and phase of complex-valued fMRI data. Neuroimage 2005;25(4):1310–24.
12. Arja SK, Feng Z, Chen Z, Caprihan A, Kiehl KA, Adali T, Calhoun VD. Changes in fMRI magnitude data and phase data observed in block-design and event-related tasks. Neuroimage 2010;49: 3149–3160.
13. Rowe DB, Nencka AS: Statistical image reconstruction of two simultaneously excited fMRI slices, Proc Am Stat Assoc, 17:201–216, 2012.
14. Rowe DB, Hyde JS, Jesmanowicz A, Nencka AS: Separation of two simultaneously encoded slices with a single coil. Proc Intl Soc Magn Reson Med, 20:123, 2013.